Title

‘Tuning’ of ribosome levels mediated by RNase I and hibernating ribosomes

Authors

Atsushi Minami[1,†], Takehito Tanzawa[2,†], Zhuohao Yang[3], Takashi Funatsu[3], Tomohisa Kuzuyama[1,5], Hideji Yoshida[4], Takayuki Kato[2], Tetsuhiro Ogawa[1,5]

Affiliations

1 Graduate School of Agricultural and Life Sciences, The University of Tokyo, Yayoi, Bunkyo-ku, Tokyo 113-8657, Japan

2 Institute for Protein Research, Osaka University, Suita, Osaka 565-0871, Japan

3 Graduate School of Pharmaceutical Sciences, The University of Tokyo, Bunkyo-ku, Tokyo 113-0033, Japan

4 Faculty of Medicine, Osaka Medical and Pharmaceutical University, Takatsuki, Osaka 569-0801, Japan

5 Collaborative Research Institute for Innovative Microbiology, The University of Tokyo, Yayoi, Bunkyo-ku, Tokyo 113-8657, Japan

† These authors contributed equally: Atsushi Minami, Takehito Tanzawa

Abstract

Ribosomes consume vast energy to synthesize proteins, so controlling the ribosome abundance is a significant concern for cells. Ribonucleases mediate ribosome degradation in response to stresses, while some ribosomes deactivate translational activity and protect themselves from degradation, called ribosome hibernation. RNase T2 is an endoribonuclease found in almost all organisms, and they are thought to be involved in the degradation of ribosomal RNA. Although it was recently reported that the activity of *Escherichia coli* RNase T2, called RNase I, depends on the environmental conditions, the regulation mechanism remains elusive. Here, we report how rRNA degradation by RNase I is regulated by hibernating ribosomes. Combining the biochemical, cryo-electron microscopy, and single-molecule analyses, we found that hibernating ribosome is an inhibitor by forming a complex with RNase I. Moreover, RNase I does not bind to the translating ribosome, so rRNA is protected. On the other hand, RNase I degrades the rRNA of each subunit dissociated from stalled ribosomes on aberrant mRNA by *trans*-translation. Under stress conditions, and even in the actively growing phase, some ribosomes are stalling or pausing. Although such ribosomes were thought to be recycled after being rescued, our results add a new insight that they are not recycled but degraded. These findings have broad implications for understanding the regulation of ribosome levels, which is critical for cellular homeostasis and response to environmental stresses.

40 **Main**

41 Ribosomes, a platform of translation, are sophisticated molecular machinery. In
42 the living cell, protein synthesis on ribosomes consumes much energy, and translational
43 activity generally depends on the number of ribosomes. Hence, the cell monitors their
44 environmental conditions and synchronizes the intracellular ribosome level. For example,
45 under stress conditions such as nutrient starvation, heat shock, or oxidative stress,
46 ribosome biogenesis and translation initiation are promptly inhibited[1]. In addition, excess
47 ribosomes are degraded[2–5].

48 On the contrary, the remaining ribosomes are protected from degradation. This
49 protection is essential for resuming protein synthesis upon recovery from stress
50 conditions. One of the protection mechanisms is 'ribosome hibernation'. This mechanism
51 also represses the translational activity of residual ribosomes to avoid energy waste[6–10].
52 In bacteria, ribosomes typically dimerize and form 100S ribosomes with the involvement
53 of hibernation-advancing factors. Several hibernation factors have been found, such as
54 RMF (Ribosome Modulation Factor), HPF (Hibernation Promoting Factor), and a newly
55 identified factor, Balon, in bacteria[6,11]; ribosome hibernation is also observed in
56 eukaryotes such as yeast and human[12,13].

57 Ribonucleases play a vital role in halting the activity of ribosomes since one of
58 the essential functions of ribosomes, peptide bond formation, is catalyzed by rRNA.
59 Among many ribonucleases, RNase T2 has been known as one of the most crucial
60 endoribonucleases degrading rRNA in various organisms[14–16]. RNase T2 was first
61 discovered in *Aspergillus oryzae*[17], and later, it was found to exist in almost all organisms.
62 It cleaves single-stranded RNA non-specifically[18], using two histidine residues as
63 catalytic residues. for example, yeast RNase T2, Rny1, degrades rRNA in the process of

64 autophagy[19,20]. The reaction mechanism consists of two steps: Firstly, the phosphodiester
65 bond is cleaved by phosphate transfer, which forms an intermediate 2′,3′-cyclic nucleotide
66 monophosphate (2′,3′-cNMPs). Subsequently, the 3′-phosphate group is formed by
67 hydrolysis.

68 While functional analysis of RNase T2 is ongoing in eukaryotes[14–16,21–23], little
69 is known about it in bacteria. Several reports have been made about *Escherichia coli*
70 RNase T2, called RNase I, which is a primary ribonuclease that degrades rRNA[24,25].
71 Moreover, it has been known to bind to the ribosomal 30S subunit[26,27], but the biological
72 significance of this interaction remains elusive. Recently, Weinert's group showed that
73 2′,3′-cNMPs, generated by RNase I, accumulate in the cytoplasm and inhibit biofilm
74 formation. Biofilms are aggregate structures of various microorganisms formed in poor
75 nutritional conditions and exposure to stress[28]. Under such conditions, the activity of
76 RNase I must be inhibited for biofilm formation. However, the regulatory mechanisms of
77 RNase I in response to its environment were utterly unknown. As described above, RNase
78 I interacts with ribosomes, which are converted into hibernating ribosomes under stress
79 conditions. Based on these facts, we hypothesized that the hibernating ribosome binds to
80 RNase I and inhibits its activity to form biofilm.

81 In this study, we demonstrated our hypothesis by investigating the inhibition
82 activity of hibernating ribosomes to RNase I *in vivo* through rRNA degradation and
83 biofilm formation *in vivo* and *in vitro*. Next, to understand the mechanism by which the
84 hibernating ribosome interacts with RNase I activity, we determined the cryo-EM
85 structure of hibernating ribosome complexed with RNase I mutant (catalytically inactive,
86 H55F/H133F) at a nominal resolution of 2.8 Å. Moreover, using single-molecule imaging
87 we revealed how RNase I discriminates between ribosomes that can bind and those that

88 cannot. Finally, we verified the state of ribosomes RNase I can degrade by biochemical
89 analyses. Taken together, the molecular mechanism and physiological significance of
90 RNase I binding to hibernating ribosomes are discussed, including molecular
91 evolutionary considerations of RNase I.
92
93 **RNase I interacts with the hibernating ribosome**
94 We first investigated whether the action of the hibernating ribosome on RNase I
95 inhibits this activity, resulting in biofilm formation in amino acid starvation condition.
96 Since RaiA, another hibernating factor in *E. coli*, is homologous with HPF, the binding
97 to ribosomes is competitive. Therefore, the RaiA-deficient strain (Δ*raiA*) highly
98 accumulates 100S ribosomes in the cytoplasm[29,30] (Extended Data Fig. 1a). These wild-
99 type, RNase I-deficient (Δ*rna*), and Δ*raiA* strains were grown under an amino acid
100 starvation condition for 4 h. The total RNA was then prepared and electrophoresed to
101 assess the extent of RNA degradation. Following the amino acid starvation, the rRNA of
102 the wild-type strain was the most degraded, approximately half that of the Δ*raiA* strain,
103 suggesting that the RNase I activity is down-regulated in the Δ*raiA* strain. In the wild-
104 type and Δ*raiA* strains, 23S rRNA was more susceptible to RNase I than 16S rRNA. On
105 the other hand, rRNA was not degraded at all; instead, it increased in the Δ*rna* strain,
106 which is consistent with previous reports[24,31–33] (Fig. 1a and Extended Data Fig. 1b). Next,
107 the biofilm-forming ability of these strains was quantified. We found that the Δ*raiA* strain,
108 like the Δ*rna* strain, showed a higher biofilm-forming ability than the wild-type strain
109 (Fig. 1b). Moreover, the high biofilm-forming ability observed in the Δ*raiA* strain was
110 reduced when RNase I was overexpressed in Δ*raiA* strain, showing that the high biofilm
111 formation observed in Δ*raiA* strain is due to the inhibition of the RNase I activity by

112 hibernating ribosomes.

113 We analyzed the interaction between RNase I and ribosomes to verify the result
114 in Fig. 1a and b. The cytoplasmic lysate was obtained from the spheroplast of *E. coli* to
115 exclude RNase I localized in the periplasm. After collecting the cytoplasmic lysate,
116 ribosomes were fractionated by ultrafiltration, followed by western blotting. As a result,
117 crude ribosome fraction extracted from the Δ*raiA* strain contained about twice as much
118 RNase I than the wild-type strain (Extended Data Fig. 2), showing that hibernating
119 ribosomes interact more readily with RNase I than 70S ribosomes. Furthermore, we
120 investigated the ability of hibernating ribosomes to inhibit RNase I activity. Δ*raiA*Δ*rna*
121 and Δ*raiA*Δ*hpf*Δ*rmf*Δ*rna* strains were constructed from the Δ*rna* strain to eliminate
122 RNase I in the cells. The Δ*raiA*Δ*rna* strain highly accumulates hibernating ribosomes in
123 the cells, whereas the Δ*raiA*Δ*hpf*Δ*rmf*Δ*rna* strain lacks all hibernating factors and,
124 therefore, does not make hibernating ribosomes. Crude ribosomes were extracted and
125 added to RNase I, and the RNase I activity was measured as the previous report[33]. We
126 found that crude ribosomes from the Δ*raiA*Δ*rna* strain inhibited RNase I activity more
127 strongly than those from the Δ*raiA*Δ*hpf*Δ*rmf*Δ*rna* strain (Fig. 1c). Together, we
128 confirmed that hibernating ribosomes interact with RNase I to inhibit its activity.
129

Fig. 1

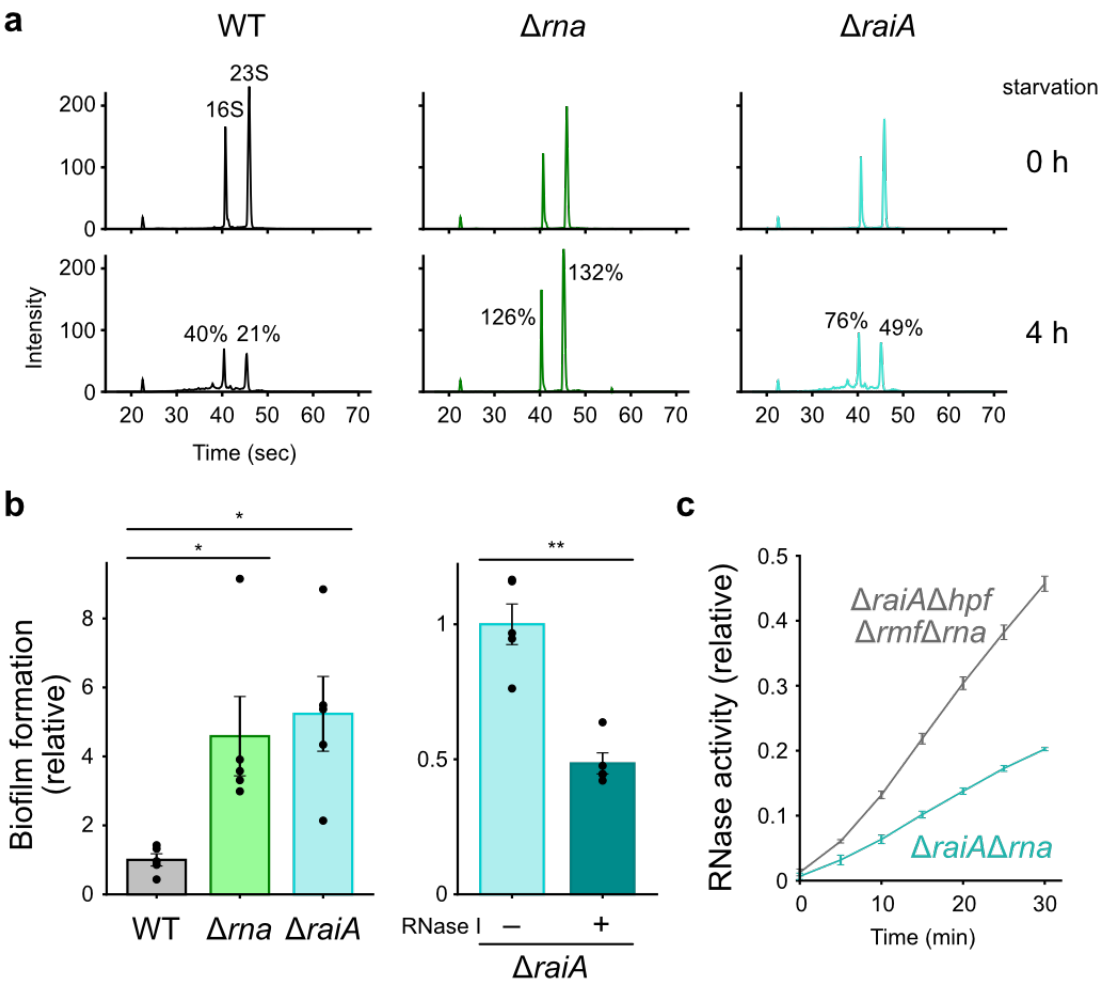

Fig. 1 | *E. coli* strain accumulating hibernating ribosomes exhibits suppression of rRNA degradation by RNase I

a, Total RNAs were extracted from indicated strains cultured before and after 4 hours of amino acid starvation, and 16S and 23S rRNA were analyzed using a Bioanalyzer. **b,** (left) The biofilm formation of *E. coli* wild-type, Δ*rna,* and Δ*raiA* strains was quantified by the crystal violet staining. (right) RNase I was overexpressed in the Δ*raiA* strain, and the biofilm formation was quantified. **c,** RNase I was added to ribosomes extracted from each strain, and the enzymatic activity of free RNase I was quantified. The experiments in **b** and **c** were five and three independent experiments, respectively, and the data are shown as the means ± standard error. Asterisks indicate significant differences (*:P < 0.05; **:P < 0.01, by Welch's t-test).

143 **Structure of hibernating ribosome and RNase I complex**

144 To unveil the mechanism of how RNase I recognizes hibernating ribosome, we
145 reconstituted the complex of RNase I H55F/H133F double mutant, which lacks the
146 catalytic activity almost completely, bound to the *E. coli* dimerized 100S ribosome. The
147 purified RNase I mutant was added to the 100S hibernating ribosomes isolated from *E.*
148 *coli* W3110 cells in the stationary phase, and the mixture was applied to the EM-grids for
149 cryo-EM observation. We collected the cryo-EM movies and operated the single particle
150 analysis of 100S•RNase complex with two or three-dimensional classification (Extended
151 Data Fig. 3). Because it has been reported that the 100S ribosome is easily split into two
152 70S ribosomes at the low concentration and that it also tends to exhibit the preferred
153 orientation on the EM-grid[30,34], we picked and extracted the RNase I-bound 70S ribosome
154 particles from micrographs, and the density map of 70S•RNase I, in which the maps of
155 both hibernation factors HPF and RMF were visible, were selected and refined. The first
156 complex chosen provided 351,633 particles, yielding a density map at a nominal
157 resolution of 2.4 Å. However, as the density of RMF was not fully occupied by this
158 complex, the 3D classification was repeated to enrich the density, finally yielding a
159 refined map to a nominal resolution of 2.8 Å consisting of 50,955 particles (Fig. 2a,
160 Extended Data Table 1, Extended Data Figs. 3, 4a and 4b).

161 The RNase I-bound hibernating complex structure revealed that the RNase I
162 binds to the surface of the head domain of the 30S subunit (Fig. 2a and Extended Data
163 Fig. 4c). As well as previous structural studies of hibernating ribosome complex, the HPF
164 interacts with the channel between the 30S head and body domains. At the same time, the
165 RMF does the anti-Shine Dalgarno (anti-SD) region between the 30S head and platform
166 domains, respectively[30,34]. The binding site of RNase I is located on the opposite side of

167 the binding regions of HPF and RMF, hence RNase I and the hibernation factors do not
168 interfere with each other (Fig. 2a). Overall, the shape of this RNase I is almost the same
169 as previous crystal structure[35]. The *E. coli* RNase I has a characteristic arch-like
170 architecture, with the active residues, H55 and H133, are located at the "keystone" of the
171 arch[35], and both ends of the arch interact with the ribosome (Fig. 2b). The active center
172 of RNase I is not in physical contact with the ribosome and is sufficiently far away from
173 the 16S rRNA, indicating that rRNA escapes degradation by RNase I (Fig. 2b). In addition
174 to helix 41 (h41) of the 16S rRNA, suggested in previous report[33], the ribosomal protein
175 uS14 interacts with the bottoms of the arch in our structure. Estimation of the binding
176 interfaces and areas obtained by PDBe-PISA[36] and APBS[37] suggest that the RNase I and
177 its binding partners are contacted mainly by electrostatic and hydrogen bonds and partly
178 by hydrophobic interactions, and that the RNase I binds primarily to the h41 and
179 secondarily to the uS14, through shape complementarity (Fig. 2c, Extended Data Fig. 5
180 and Extended Data Table 2).

181 The stem-loop A1257–G1278 of h41 binds by bridging both arch bottoms of the
182 RNase I (Fig. 2b and Extended Data Fig. 5). The polar amino acid residues R31, R33,
183 Q198, and N233 of the RNase I form hydrogen bonds with the nucleotides G1272–A1274
184 in the h41 stem region. The binding residues of RNase I do not recognize the groove of
185 the mini-helix formed by G1272–A1274 and their base-pair partners, but take advantage
186 of the arch-shaped features of RNase I to bind only one bank of the groove (Fig. 2c and
187 2d [h-(i)]). In the other binding region, the RNase I recognizes A1257 and G1278 at the
188 kink of the h41 stem. This kink does not give both bases any base-pairing partners and
189 leaves them free, allowing the RNase I to stabilize on the stem-loop. The R83 mainly
190 forms hydrogen bonds with both A1257 and G1278 and exhibits stacking interactions

191 with the base of A1257 (Fig. 2c, 2d [h-(ii)]). Interestingly, compared to a typical *E. coli*
192 70S ribosome[38], RNase I binding causes the A1257 to rotate approximately 100 degrees
193 to the h41 stem-loop side to avoid collision with the R74 (Fig. 2e). This conformation
194 forms a pseudo-major groove consisting of A1257–G1260 and A1274–G1278, where
195 helix α4 of the RNase I is placed in a shape complementary manner (Fig. 2d [h-(ii)] and
196 Extended Data Fig. 6). In detail, the F78 has a π-stacking interaction with the base of
197 A1257 at the other side of R83, and the R73 and R74 make hydrogen bonds with its main
198 chain (Fig. 2d [h-(ii)]). The conformational change of A1257 by the recruiting to RNase
199 I promotes the loss of interaction between A1257 and F21 of uS14 (Fig. 2e), and the cleft
200 created by this local dissociation between h41 and uS14 is filled by the R74 of RNase I
201 (Fig. 2d [s-(i)]). Thereby, the R74 recognizes the F21 instead of the A1257, also the loop
202 containing G69–D71 of RNase I contacts the residues D18–A22, located in the bent of
203 the N-terminal helix of uS14 (Fig. 2b, 2d [s-(i)]). As well as h41, the N-terminal helix
204 also binds to bridge both arches of the RNase I, with another binding site on the opposite
205 side of the above (Fig. 2b and Extended Data Fig. 5). The residues P229–P231 in the
206 Pro/Gly-rich long loop between β5 and β6 of RNase I exhibit electrostatic interactions
207 with the residues I30–N35 of uS14, with hydrogen bond between the H230 and D33 (Fig.
208 2c, 2d [s-(ii)]). Collectively, our structure of the RNase I•hibernating ribosome complex
209 provides an understanding of the unique interaction mechanism, allowing hibernating
210 ribosomes to protect themselves from degradation by RNase I.

Fig. 2

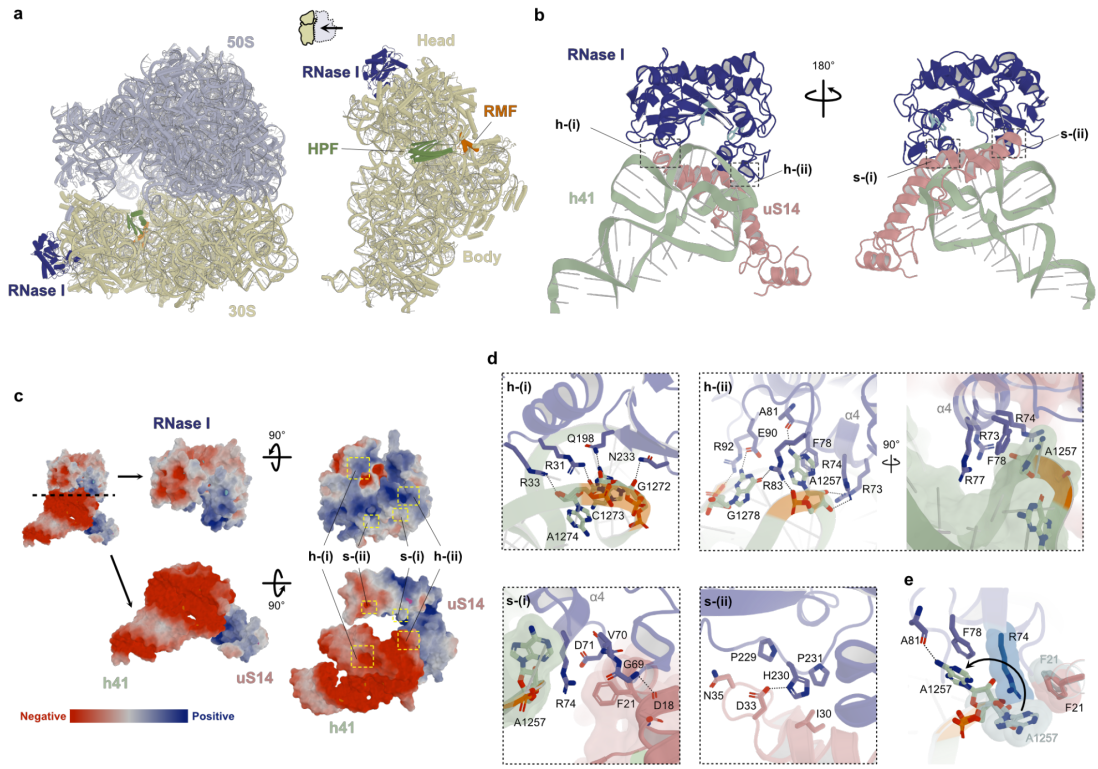

Fig. 2 | Structure of the RNase I-bound hibernating ribosome complex. **a,** Overall view of the RNase I-bound hibernating ribosome showing the structure of the *E. coli* 70S ribosome in complex with RNase I (dark blue), HPF (green), and RMF (orange). The 50S subunit is shown in light blue and the 30S subunit in light yellow (left panel). Overview from a different angle with the 50S subunit omitted for clarity (right panel). **b,** Close-up view of the interaction between the RNase I and the h41 (light green) of the 16S rRNA or the ribosomal protein uS14 (light pink), viewed from two different angles. The black dashed rectangles indicate the estimated binding interfaces between RNase I and h41 or uS14 calculated using PDBe-PISA. The h41 and uS14 interact at both ends of the arch architecture of the RNase I, respectively, and these are shown by h-(i) and h-(ii) for h41 and s-(i) and s-(ii) for uS14. **c,** The electrostatic potential surface of the RNase I, h41, and uS14 as a single mass is shown from the same direction as **b**. The mass is split into the RNase I and h41•uS14, each viewed from two different perspectives. Both positive, negative, and neutral electrostatic surface potentials are shown in blue, red, and white. The yellow dashed rectangle illustrates each binding region. **d,** Detailed views of the major binding regions of RNase I to h41 (h-(i) and h-(ii)) or uS14 (s-(i) and s-(ii)). Chains of RNase I, h41, and uS14 are colored the same as **b**. Stick models represent amino acid residues and nucleotides involved in these bindings, and the N, O, and P-atom are colored

blue, red, and orange, respectively. Dashed lines indicate hydrogen bonds. **e,** Structural comparison of the A1257 of h41 and the F21 of uS14 by superposing the stem-loop of h41 between RNase I bound hibernating complex and a typical 70S ribosome (PDB 8SYL). The 8SYL ribosome is colored by whitish blue and the ternary complex is shown in the same as **b**. The base of A1257 (PDB 8SYL) and the side chains of R74 (RNase I) and F21 (our model and PDB 8SYL) are represented by stick and sphere models. The curving arrow illustrates the rotation of the A1257 base.

242 **RNase I does not interact with the translating ribosome**

243 Our *in vivo* binding assay showed that RNase I interacts with hibernating
244 ribosomes more tightly than 70S ribosomes, and the cryo-EM structure revealed the
245 interaction mechanism between RNase I and ribosomes. However, the *in vitro* binding
246 assay of hibernating ribosomes, reconstituted by adding RMF and HPF (hereafter referred
247 to as "HFs") and 70S ribosomes almost comparably bound to RNase I mutant (Fig. 3a,
248 b). The binding affinity of RNase I to ribosomes decreased in the exponential phase
249 (Extended Data Fig. 2), where most ribosomes are engaged in translation. Given these
250 results, we assumed that RNase I cannot interact with the translating ribosomes. We then
251 performed the binding assay between RNase I and translating ribosomes *in vitro* using
252 the PURE system[39], the reconstituted translation system derived from *E. coli*. Translating
253 ribosomes had a reduced ability to interact with RNase I compared to the non-translating
254 70S ribosomes or reconstituted hibernating ribosomes (Fig. 3c).

255 It is known that not all ribosomes are engaged in translation; instead, limited
256 ones synthesize proteins in an *in vitro* translation such as the PURE system. We
257 considered that this fact might influence our experimental results. Therefore, we
258 performed a single-molecule imaging method to solve this issue. In recent years, several
259 groups have developed real-time imaging techniques of translation at the single-molecule
260 level[40–43]. In the experimental system, multi-epitope protein tags are translated on the
261 ribosome, and fluorescently labeled antibodies recognize and bind to the tags, enabling
262 the translational visualization of ribosomes. However, almost all single-molecule imaging
263 methods are performed in mammalian cells. To our knowledge, only one *in vitro*
264 experiment has been reported using yeast lysate.

265 Here, we attempted to perform antibody-based single-molecule translation

266 imaging *in vitro* using the PURE system. This allowed real-time translation and binding
267 of RNase I to the ribosome at the single-molecule level. The experimental design is
268 summarized in Fig. 3d. A single ribosome particle was defined as a spot where mRNA-
269 derived fluorescence was observed. Here, a fluorescently labeled nanobody, a small
270 single peptide recognizing multi-epitope protein tags, is used instead of whole antibodies
271 or Fab fragments. Nanobody-derived fluorescence appeared in some ribosome particles,
272 indicating that translation elongation was in progress ("translating region"). In other
273 regions, ribosomes remain arrested as nanobody-derived fluorescence was not observed
274 ("arrested region"). Instead, RNase I mutant (H55F/H133F)-derived fluorescence was
275 observed, and fluorescence of nanobody and RNase I were never detected in the same
276 spot (Fig. 3e). Together, we could observe that RNase I does not interact with translating
277 ribosomes as a single-molecule level. Notably, spots of RNase I-derived fluorescence
278 observed in the arrested region were not retained long; most of RNase I was released
279 within 1 or 2 min (Fig. 3f), indicating that RNase I may be unable to maintain a stable
280 interaction with ribosome.

Fig. 3

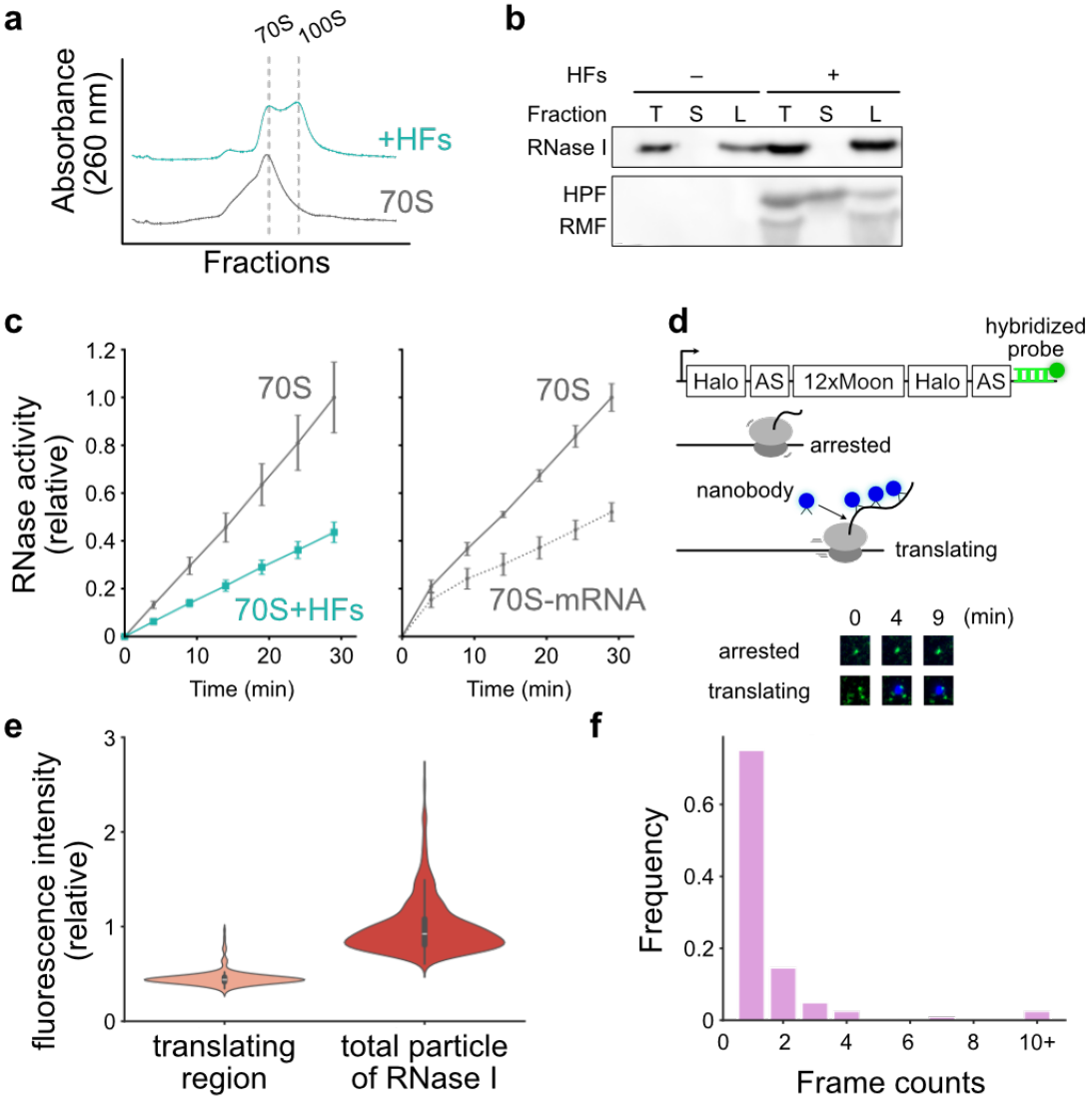

Fig. 3 | RNase I binds to 70S and 100S ribosomes but does not bind to translating 70S ribosomes.

a, HFs were added to 70S ribosomes, and 70S and 100S ribosomes were detected using sucrose density gradient centrifugation. **b,** RNase I (H55F/H133F) was added to the ribosome with or without hibernation factors. Mixtures were fractionated by ultrafiltration with a 300 kDa cut-off. RNase I remained in the large fraction and was detected by western blotting. “T” indicates the total mixtures, and “L” indicates the large fraction, while “S” indicates the small fraction. **c,** RNase I was added during translation using an *in vitro* reconstituted translation system. Mixtures were fractionated as described in **(b)**, and the enzymatic activity

of RNase I that did not bind to ribosomes was detected in Fig. **1(c)**. The enzymatic activities of RNase I were compared between when RNase I was added to translating ribosomes (black, solid line) and to ribosomes with added HFs (blue, solid line) (left) or to not translating ribosomes (black, dashed line) (right). Data are presented as the means ± standard error of 3 independent experiments. **d,** (upper) Schematic depicting the experiments performed in **(e)** and **(f)**. The template mRNA is marked by the oligo DNA probe that hybridizes to repeated sequences located in 3′ end (green). At the start of the observation, the mRNA and the ribosome complex is fixed on the glass base via HaloTag. The ribosome is arrested on the mRNA due to the SecM arrest sequence (AS), so labeled RNase I mutant can bind to the ribosome (“arrested”). After the arrested ribosome is released, the nascent polypeptide chain is labeled by nanobodies (blue) that bind to peptide epitopes, MoonTag (“translating”). (lower) Example co-localization of nanobodies-bound nascent chain and mRNA. **e,** The RNase I-derived fluorescence intensity distribution at the coordinates where translation spots were observed and the overall fluorescence intensity of the RNase I-derived spots. The vertical axis is the relative value with the mean of the overall fluorescence intensity of the entire RNase I-derived fluorescence spot (right) as 1. **f,** RNase I-derived fluorescence spots localized in the “arrested” regions were detected, and the number of consecutive frames detected was counted. The frame interval is approximately 1 minute.

315 **RNase I degrades rRNA within dissociated ribosomal subunits derived from *trans*-**
316 **translation**

317 Finally, we considered how RNase I cleaves rRNA to produce 2′,3′-cNMPs in
318 cells. The previous report showed that 2′,3′-cNMPs were detected during the actively
319 growing phase[44]. However, it is known that the 70S ribosome is highly resistant to
320 RNases[45]. Indeed, RNase I hardly degraded the rRNA in equimolar amounts with the
321 ribosomes *in vitro* (Fig. 4b). This low susceptibility of rRNA to RNases is due to
322 ribosomal proteins wrapping around the rRNA, which results in protecting rRNA from
323 degradation[46]. As shown above, our results indicate that the target of RNase I is non-
324 translating ribosomes; however, RNase I cannot attack rRNAs within 70S ribosomes.
325 Then, how does RNase I degrade the rRNA of non-translating ribosomes? Compared to
326 our complex structure, we found that the RNase I bound to the ribosome spatially shares
327 a region with a large pseudoknot ring (PK ring) of transfer-messenger RNA (tmRNA)
328 (Fig. 4a). In bacteria, *trans*-translation is one of the primary 'rescue system' for ribosomes
329 stalled on mRNA, mediated by tmRNA and small protein B (SmpB). The tmRNA is
330 composed of a PK ring, a tRNA-like domain (TLD), and a mRNA-like domain (MLD),
331 and it enters the vacant A-site of ribosomes stalled at the 3′ ends of mRNA, which lacks
332 a stop codon. Then, a degradation tag, encoded by the MLD, was added to the C-terminus
333 of a nascent polypeptide chain, thereby degrading the synthesized polypeptide. In
334 addition, the stalled ribosomes are split into the 30S and 50S subunits, resulting in release
335 from the aberrant mRNA[47]. Taken together, we hypothesized that RNase I could
336 cooperate with tmRNA to degrade rRNA within the split ribosomal subunits.

337 To validate the hypothesis that rRNAs within split ribosomal subunits become
338 susceptible to RNase I, we separated the ribosome into the 30S and 50S subunits[48] and

339 then incubated with RNase I. As expected, rRNAs of subunits were more degraded by
340 RNase I than that of 70S ribosomes (Fig. 4b). Even in the actively growing phase, a
341 certain number of ribosomes are stalled on mRNA, e.g., due to aberrant mRNA or
342 ribosomes[49], resulting in the generation of 2′,3′-cNMPs. Notably, the rRNAs were
343 fragmented by the degradation, suggesting that the first cleavage by RNase I may have
344 occurred in the helix 69 (h69) of 23S rRNA[50]. If this assumption is correct, a fragment of
345 approximately 1900 nt should accumulate, roughly consistent with the fragment length
346 visualized by electrophoresis shown in Fig. 4b.

347 Amino acid starvation also induces intracellular accumulation of 2′,3′-cNMPs[44];
348 that is, RNase I degrades rRNA. However, ribosomes are engaged in translation, as cells
349 proliferate even under such condition, albeit at a reduced growth rate. During amino acid
350 starvation, ribosomes are generally prone to stall and resume translation repeatedly[51,52].
351 Swivels in the head domain, where RNase I has been found to bind, are important in
352 translation. Therefore, we surmised that the binding of RNase I to the head domain
353 interferes with translation. Thus, we measured the translational activity of RNase I-bound
354 ribosomes. Ribosomes and RNase I mutant (H55F/H133F) were mixed *in vitro*, and
355 translation was initiated using the PURE system (Fig. 4c). As a result, the translational
356 activity was critically reduced when RNase I was added before translation initiation.
357 Although inhibition of translation initiation by RNase I seems to be beneficial for *trans*-
358 translation as tmRNA acts on ribosomes stalled on mRNA, our complex structure
359 suggests that RNase I and tmRNA spatially share a binding region as described above
360 (Fig. 4a). We measured *in vivo trans*-translation activities in the presence or absence of
361 RNase I to verify the result obtained from the cryo-EM analysis. Here, *trans*-translation
362 was induced by expressing a gene encoding mRNA lacking the stop codon of GFP and

363 transcribing a tmRNA mutant that adds a non-degradation tag to the nascent polypeptides.
364 Then, *trans*-translation activity can be quantified by measuring the GFP fluorescence.
365 Consequently, *trans*-translation activity increased in the RNase I-deficient strain,
366 indicating that binding sites of RNase I and tmRNA are overlapped (Fig. 4d). As
367 mentioned, subunit dissociation by *trans*-translation is required for the rRNA degradation
368 by RNase I. However, if RNase I continues to interact with the head domain stably, the
369 efficiency of tmRNA entering the A-site will severely decrease, and RNase I will never
370 produce 2′,3′-cNMPs. Considering that RNase I efficiently degrades rRNAs under amino
371 acid starvation condition (Fig. 1a, Extended data Fig. 1b), the binding of RNase I to the
372 head domain is not so stable, which is consistent with the results arose from the single-
373 molecule imaging that RNase I binding with the ribosome is transient (Fig. 3f). Taken
374 together, we concluded that this transient binding allows tmRNA to enter the ribosomal
375 A-site, leading to RNase I degrading rRNA in the subunit after the dissociation by *trans*-
376 translation.
377

Fig. 4

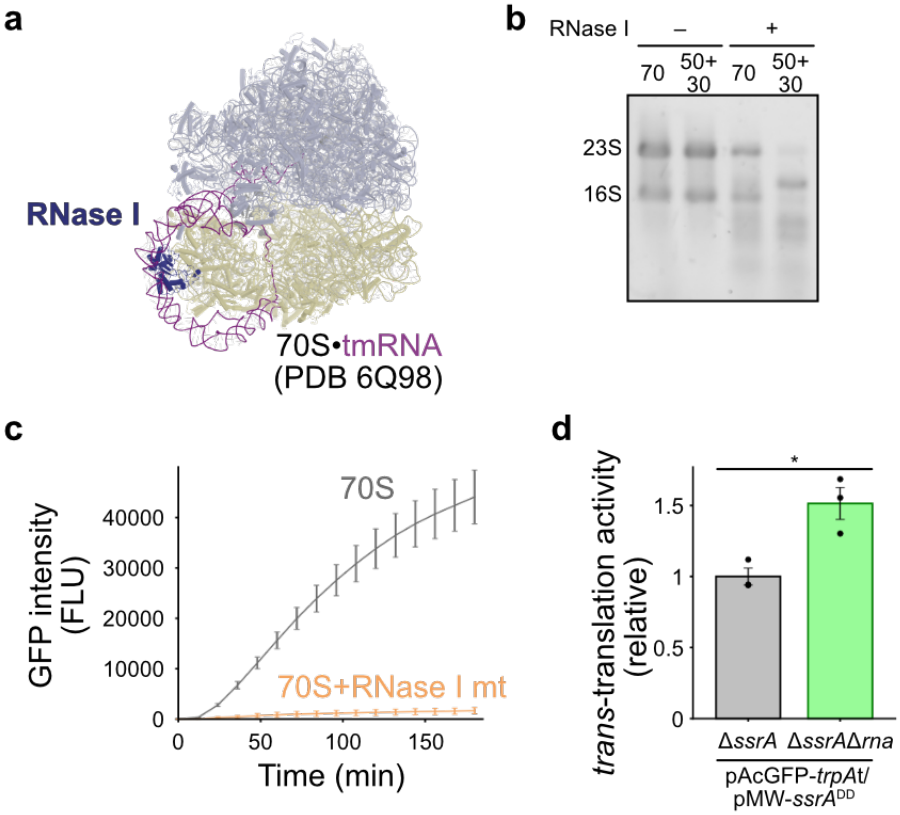

Fig. 4 | RNase I degrades rRNA from subunits dissociated by *trans*-translation.
a, The hibernating ribosome•RNase I complex and the trans-translating 70S•tmRNA complex (PDB 6Q98) were superposed by 70S, based on the interaction sites shown in Fig. 2. The PK ring of tmRNA extends outside the head domain of the 30S subunit, which spatially overlaps with RNase I. **b,** The 30S/50S subunits dissociated by adding a dissociation buffer to 70S ribosomes, and 70S ribosomes were prepared. Total RNAs were extracted from each of them after incubation with or without RNase I, and electrophoresed using a formalin-denaturing gel. “70” indicates rRNAs from intact 70S ribosomes, while “50+30” indicates rRNAs from dissociated subunits. **c,** RNase I mutant was added at the beginning of *in vitro* translation, and the translational activity was measured. **d,** The *trans*-translation activities in the Δ*ssrA* strain and the Δ*ssrA*Δ*rna* strain carrying the two plasmids (see Methods) were compared. Data are presented as the means ± standard error of 3 independent experiments. Asterisks indicate significant differences (*:P < 0.05, by Welch’s t-test).

395 **Discussion**

396 Ribosome degradation and protection are central concerns for all living things,
397 especially under stress conditions. In *E. coli*, RNase I is the most critical ribonuclease in
398 the mechanism for the control of intracellular ribosome levels. Although RNase I was
399 discovered over 60 years ago, its regulatory mechanism has been poorly understood. This
400 study shows the specific interaction between RNase I and hibernating ribosomes to inhibit
401 RNase I activity under stress conditions. These results explain the biological significance
402 of the past findings on why RNase I binds to the 30S subunit[26,27]. As mentioned,
403 hibernating ribosomes protect themselves from the attack of RNase I. However,
404 hibernating ribosomes are gradually degraded after prolonged exposure to stresses[29].
405 Therefore, the biological significance of interactions between RNase I and hibernating
406 ribosomes may be not only in the inhibition of RNase I activity but also in rRNA
407 degradation under prolonged stresses. Fessler *et al*. demonstrated that rRNA is degraded
408 by several starvation conditions and suggested that phosphate and nucleotides are
409 recycled[53]; this is consistent with our results that RNase I degrades hibernating ribosomes
410 when cells are exposed to long-term stresses (Extended Data Fig. 1b). In addition, our
411 result indicated that RNase I degrades rRNA to several fragments (Fig. 4b). It has been
412 suggested that these rRNA fragments are ultimately degraded by the exoribonucleases
413 RNase R or PNPase[45], whose product may be utilized to survive prolonged nutrient
414 starvation.

415 Our study indicated that rRNA degradation by RNase I, responsible for the first
416 step for degradation (Fig. 1a, Extended Data Fig. 1b), targets the stalled ribosome on the
417 aberrant mRNA. Such stalled ribosomes are possible to induce ribosome collision[54].
418 SmrB in *E. coli* was recently found to cleave mRNA upstream of collided ribosomes,

419 enabling *trans*-translation[55]. Furthermore, ribosome dissociation into ribosomal subunits,
420 commonly referred to as ribosome rescue, is required for the rRNA degradation by RNase
421 I. This study provides an opportunity to reconsider whether ribosomes are 'recycled' after
422 *trans*-translation. To our knowledge, no reports show that ribosomes rescued from mRNA
423 by *trans*-translation are recycled. On the other hand, a mechanism called nonfunctional
424 rRNA decay (NRD)[56,57], which is present not in bacteria but in eukaryotes, recognizes
425 and degrades stalled ribosomes during the translation initiation or elongation. Our
426 research proposes a model in which the rescued ribosomes are degraded rather than
427 recycled, similar to NRD. Moreover, taking into account that RNase I can only bind to
428 stalled ribosomes and that RNase I-bound ribosomes cannot initiate translation, we
429 further extend the existing molecular mechanism of ribosome rescue (Fig. 5b). Even
430 during the exponential phase, some ribosomes are stalled on mRNA for various reasons,
431 such as damage to rRNA or the absence of stop codons on mRNA. Our results indicate
432 that RNase I needs to leave the ribosome for tmRNA to enter the ribosomal A-site. One
433 possible reason why RNase I binds to the 30S ribosomal subunit is that it gathers near
434 arrested ribosomes, which are dissociated to each subunit by *trans*-translation, allowing
435 RNase I to degrade rRNA in dissociated subunits efficiently. This assumption seems
436 reasonable given the intracellular ratio of ribosomes to RNase I. The location where
437 RNase I binds may be coincidentally suitable for destabilizing RNase I binding by turning
438 the head domain, although this could not be proven experimentally. Rare codons on the
439 mRNA reduce the translation elongation rate while it does not stall the ribosome
440 completely. It may be possible that RNase I binds to these ribosomes, which results in the
441 inhibition of translation initiation as the presence of a rare codon induces *trans*-
442 translation[58].

Fig. 5

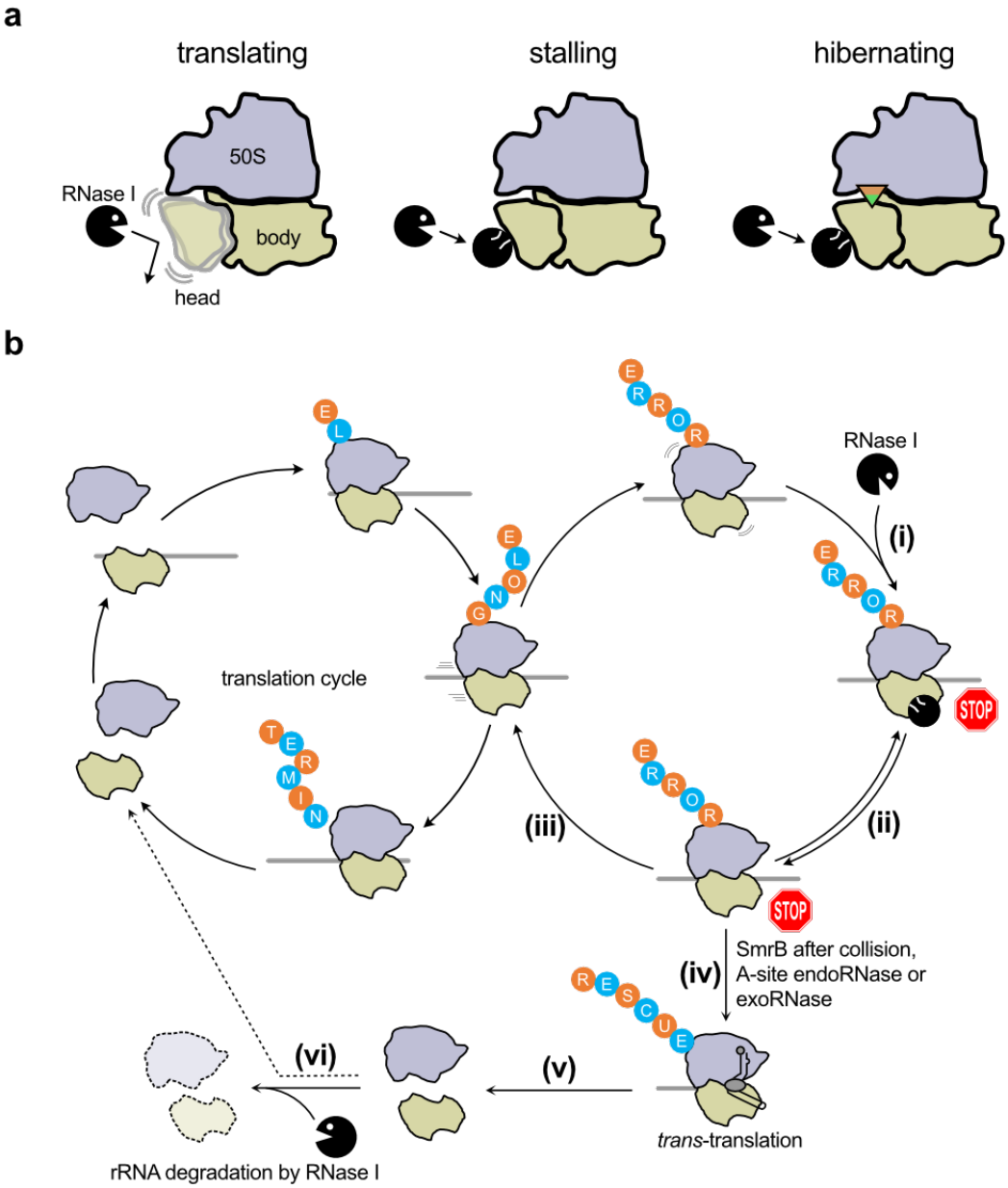

Fig. 5 | Model of the interaction between RNase I and ribosomes. **a,** When the ribosome is translating, the 30S head domain rotates relatively to the body, called "swivel," so the interacting site of RNase I is unstable (left). On the other hand, the domain in the stalled ribosome (center) or hibernating ribosome (right) is stable, so RNase I easily binds to the ribosome. **b,** Extended Model of ribosome recycling and RNase I-mediated rRNA degradation. RNase I binds to abnormally arrested ribosomes that occur at a specific rate during

translation **(i)**. Binding at this point is also thought to play a role in completely stopping translation by binding to ribosomes that are prone to stall. However, the binding affinity of RNase I to the arrested ribosome is not so high, and the binding and dissociation are thought to be repeated **(ii)**. The stably stopped ribosome may return to the normal cycle of translation **(iii)**, but with the help of some RNase, tmRNA can act on the arrested ribosome (**iv**), and the ribosome is rescued and split **(v)**. Those split ribosomal subunits were thought to be reused for translation, but RNase I can degrade the dissociated ribosome-derived rRNA after *trans*-translation **(vi)**.

461 RNase I localizes mainly in the periplasm, but the biological role of the
462 localization is still unknown. One possible physiological significance of RNase I
463 accumulating in the periplasm lies in oxidative folding, as RNase I has four disulfide
464 bonds[59,60]. As described, RNase I degrades rRNA in the cytoplasm (Fig. 1a and Extended
465 Data Fig. 1b). However, the mechanism which RNase I, generally localized in the
466 periplasm, enters the cytoplasm is unclear. Previous reports discussed the entrance of
467 RNase I in the cytoplasm by such as changes in cell membrane permeability and
468 involvement of F factor-derived toxin, SrnB[61,62]. Further verification is needed to
469 determine the cause of RNase I influx into the cytoplasm.

470 One of the most remarkable findings in the present study is the elucidation of
471 where and how RNase I interacts with the hibernating ribosome. Our cryo-EM structure
472 shows that the RNase I binding region is located on the head domain of the 30S subunit,
473 which constantly fluctuates during translation due to swivel and rotation. In contrast, the
474 head domain becomes stable when the ribosome stops translating or transits the
475 hibernation state (Fig. 5a). In particular, the early cryo-EM study showed that h41, to
476 which RNase I binds, rotates approximately 10 degrees during EF-G•GTP-mediated
477 ratchet rotation[63]. As a result, translation may reduce the structural and thermodynamic
478 stabilities of the head domain, destabilizing the interaction with RNase I. Moreover, the
479 molecular dynamic simulation of the translation initiation complex predicted that the
480 region of C1254-C1284 of h41 would undergo conformational changes[64]. Together with
481 our results (Fig. 4c), the fluctuation of the 30S head may be suppressed in RNase I-bound
482 ribosomes, resulting in the inhibition of translation. Moreover, the RNase I interacts with
483 the uS14, which may be vital to unlocking the diverse functionality and evolutionary
484 significance of the uS14 protein. Despite the gene for uS14 being essential, the function

485 of uS14 in translation remains elusive. The uS14 protein is classified into three groups
486 according to the presence or absence of a zinc-binding motif, and *E. coli* uS14 belongs to
487 the C- long type[65]. Compared to the crystal structure of uS14 in *Thermus thermophilus*
488 70S ribosome (PDB 4V8H[34]) , which belongs to the C+ type, *E. coli* uS14 has a distinctive
489 domain with an internal insertion containing the contact site to RNase I (Extended Data
490 Fig. 7a). No homologous protein of RNase I has been found in *T. thermophilus*,
491 suggesting that *E. coli* uS14 may have evolved independently, along with its interaction
492 with RNase I. In addition, C+/- paralogue pairs for uS14 are conserved in some bacteria,
493 and their functionality differences have been reported[65–67]. These results support that
494 uS14 is a susceptible region in the evolutionary process for gaining diverse functions.

495 RNase I shows the diversity of their sequences and structures among species.
496 The RNase T2 family exists in a wide range of species, as mentioned above. We focused
497 on *E. coli* RNase I in this study, and previously, we reported on *Saccharomyces cerevisiae*
498 RNase T2, Rny1[20]. In that study, molecular phylogenetic analysis of RNase T2 shows
499 that fungal RNase T2 evolved independently from other species in the early stage of
500 evolution. Moreover, it was also suggested that *E. coli* RNase I also evolved apart from
501 mammals and plants. We thus compared the structure of *E. coli* RNase I with that of
502 human RNase T2 (PDB 3T0O[68]). Then, we found a region-specific to *E. coli* RNase I,
503 which is one of the binding sites to the ribosome (Extended Data Fig. 7b). This may mean
504 that during the evolution of bacteria, RNase I acquired its binding function to the
505 ribosome. Together with the diversity of uS14, RNase I and ribosomes have evolved to
506 'checkmate' each other by the interaction. In particular, the structure of ribosomes is often
507 highlighted for its commonality between species, but many areas differ between species;
508 ribosomes have likely optimized their structures in response to their relationship with

509 trans-acting diverse protein factors, such as RNase I and hibernation factors.

510 Recently, it was reported that the RNase R binds to the 30S platform to proceed
511 with degrading the anti-SD and the helix 44 at the decoding center using cryo-EM single
512 particle analysis[69]. Compared with our structure of the RNase I•hibernating ribosome
513 complex, the binding region of RNase R is entirely different from that of RNase I. Rather,
514 it overlaps in that of the hibernation factor RMF (Extended Data Fig. 7c), indicating that
515 hibernating ribosomes also inhibit the activity of RNase R in *E. coli*[9]. Our research
516 revealed that the inhibitory mechanism of RNase I by hibernating ribosomes is also quite
517 different from that of RNase R, in which hibernating ribosomes bind directly to RNase I,
518 thereby keeping it away from its active site. This suggests that hibernating ribosomes
519 have acquired multiple protection mechanisms to resist the attacks of diverse intracellular
520 ribonucleases.

521

522 **Methods**

523 ***Construction of strains and plasmids***

524 The strains and plasmids used in this study are listed in Supplementary Table S1.
525 The RNase I, RaiA, RMF, or HPF-deficient strains (Δ*rna*, Δ*raiA*, Δ*rmf*, or Δ*hpf*,
526 respectively) were obtained from the Keio Collection, which was provided by the
527 National BioResource Project (NBRP) at the National Institute of Genetics, Japan[70]. The
528 kanamycin-resistance gene of strains from the Keio Collection was eliminated by
529 homologous recombination using plasmid 707-FLPe (Gene Bridges). The double mutant
530 strain (Δ*raiA*Δ*rna*) or quadruple mutant strain (Δ*raiA*Δ*hpf*Δ*rmf*Δ*rna*) were produced by
531 homologous recombination using the Red/ET system.

532 The open reading frame (ORF) and the promotor region of the *rna* gene were
533 PCR-amplified from *E. coli* genomic DNA extracted from BW25113 wild-type strain and
534 inserted into the pUC18 vector with the seamless cloning method (In-Fusion HD Cloning
535 Kit, TaKaRa Bio). For the expression of recombinant RNase I wild type and mutants,
536 RMF, HPF, and the nanobody of MoonTag, PCR-amplified ORFs were inserted into the
537 pET24d(+) vector with the same method. The plasmid coding the nanobody of MoonTag
538 was kindly gifted by Dr. Wataru Fujii (The University of Tokyo, Japan). The plasmid
539 pET-*gfp* was created in this study to measure the *in vitro* translation activity. The plasmid
540 pMW-*ssrA*^{DD} expressing mutant tmRNA was kindly gifted by Dr. Hyota Himeno
541 (Hirosaki University, Japan). The plasmid harboring the *trans*-translation inducing
542 sequence was created as follows: First, the ampicillin resistance cassette of pAcGFP1
543 plasmid purchased from TaKaRa Bio was replaced with the kanamycin resistance cassette
544 by the seamless cloning method. Next, the stop codon of the ORF was replaced with the
545 *trpA* terminator sequence using the same method. The resulting plasmid was designated

546 pAcGFP-woSTOP-*trpAt*. The template sequence for the single-molecule imaging was
547 created as follows: First, the template 12xMoonTag-12xSunTag-kif18b-24xPP7 was
548 purchased from Addgene (#128606)[71]. Second, the HaloTag-SecM sequence was inserted
549 into the spacer region between 12xMoonTag and 12xSunTag by the seamless cloning
550 method (NEBuilder HiFi DNA Assembly, NEB). Third, the plasmid was digested with
551 NcoI and ApeI, and inserted into pET24d(+). Subsequently, PCR-amplified HaloTag-
552 L26-SecM$^{133-170}$ sequence[72] was inserted between the start codon and 12xMoonTag of
553 the plasmid.

554 ***Preparation of RNase I, hibernation factors***

555 *E. coli* BLR(DE3) strain transformed with the expression plasmids were grown
556 in the lysogeny broth (L-broth) supplemented with 30 μg/mL of kanamycin. When an
557 OD_{660} reached 0.5, isopropyl β-D-1-thiogalactopyranoside (IPTG) was added to the
558 culture at a final condition of 1 mM to induce the expression of RNase I wild type and
559 mutants, RMF, and HPF, and the culture was further incubated for 3 h at 37 °C. The
560 purification of RNase I wild type and mutants was performed as described[20] with slight
561 modifications. The cells were harvested by centrifugation, and the cell pellet was
562 resuspended in 20 mL of lysis/wash buffer (20 mM Tris-HCl (pH 7.5), 500 mM NaCl,
563 and 20 mM imidazole (pH 8.0)), followed by sonication on ice to lyse the cells. Cell
564 debris was removed by centrifugation at 17,000 rpm for 20 min. The supernatant was
565 applied to the Ni-NTA column, and the resin was washed with 20 mL of lysis/wash buffer.
566 Then, RNase I was eluted in 5 mL of elution buffer (20 mM Tris-HCl (pH 7.5), 500 mM
567 NaCl, and 250 mM imidazole (pH 8.0)). The purified RNase I was concentrated using a
568 Vivaspin 20 device (10,000 MWCO; Sartorius) and stored in the storage buffer (20 mM
569 Tris-HCl (pH 7.5), 50 mM NaCl)[60]. For the purification of RMF and HPF protein, lysis

570 buffer (20 mM Tris-HCl (pH 7.6), 100 mM NH_4Cl, 10 mM $MgCl_2$, 1 mM β-
571 mercaptoethanol), wash buffer (20 mM Tris-HCl (pH 7.6), 1 M NH_4Cl, 10 mM $MgCl_2$, 1
572 mM β-mercapthoethanol), elution buffer (20 mM Tris-HCl (pH 7.6), 100 mM NH_4Cl, 10
573 mM $MgCl_2$, 2 M imidazole (pH 8.0), 1 mM β-mercapthoethanol), and storage buffer (20
574 mM Tris-HCl (pH 7.6), 100 mM NH_4Cl, 10 mM $MgCl_2$)[34] was used instead of each buffer
575 described above. For the purification of RMF protein, an equal volume of 2 M LiCl was
576 added to the supernatant after sonication and stirred overnight at 4 °C, followed by
577 elution[73].

578 ***Isolation of ribosomes and sucrose density gradient centrifugation analyses***

579 *E. coli* 70S ribosomes were prepared from the Δ*raiA*Δ*hpf*Δ*rmf*Δ*rna* strain as
580 described[74]. *E. coli* 100S ribosomes for the sucrose density gradient centrifugation
581 (SDGC) analysis, the cell pellets were resuspended in 1 mL of the ribosome gradient
582 buffer (20 mM Tris-HCl (pH 7.5), 60 mM NH_4Cl, 7.5 mM $Mg(OAc)_2$, 0.5 mM EDTA, 6
583 mM β-mercaptoethanol)[75] and disrupted by shaking for 5 min with 300 mg of zirconium
584 silicate beads in a homogenizer (ShakeMaster Neo, Bio Medical Science Inc.). The
585 sample was then centrifuged for 10 min at 18,500 g and 4 °C, and the resultant supernatant
586 was collected. The absorbance at 260 nm (A_{260}) for lysates was determined by Nanodrop,
587 and 300 μL of normalized lysate was loaded on a 10% to 40 % sucrose gradient in the
588 ribosome gradient buffer. After 3 h of centrifugation at 35,000 rpm and 4 °C in a Beckman
589 SW41 rotor, the sample was collected with a BioComp gradient station monitoring
590 continuous absorbance at 254 nm. The *in vitro* reconstituted hibernating ribosomes were
591 prepared by incubating 23 pmol of 70S ribosomes with 240 pmol of RMF and 830 pmol
592 of HPF in the reaction buffer (20 mM Tris-HCl (pH 8.0), 100 mM NH_4Cl, 10 mM $MgCl_2$)
593 for 30 min and 37 °C. The SDGC analysis profiled the resulting mixture as above.

594 ***Extraction of total RNA from E. coli cells***

595 *E. coli* each strain was cultivated in L-broth until an OD_{660} reached 0.5. The
596 medium was changed to M9 minimum medium (supplemented with 0.4% glucose and
597 0.2% casamino acids) and further cultivated for 2 or 4 h. The cells were subsequently
598 collected, and total RNA was extracted using an RNeasy Mini Kit (QIAGEN). The
599 extracted total RNA was analyzed with electrophoresis using MOPS-formaldehyde
600 denaturing gel or a Bioanalyzer (Agilent).

601 ***Quantification of biofilm formation activity***

602 Biofilm formation was quantified by crystal violet staining following a published
603 procedure[76].

604 ***Preparation of 100S ribosomes for cryo-electron microscopy***

605 *E. coli* W3110, a wild-type K-12 strain, was used to prepare 100S ribosomes.
606 Overnight 2-mL precultures were obtained in medium E containing $MgSO_4$, citric acid,
607 K_2HPO_4, and $NaNH_4HPO_4$, and were supplemented with 2% polypeptone and 0.5%
608 glucose at 37 °C with shaking at 180 cycles per minute[77]. Mass cultures were performed
609 in 100 mL of the same medium at 37 °C, shaking at 130 cycles per minute. The cells were
610 harvested 24 h after the start of mass culture. The harvested cell pellets were suspended
611 in an association buffer [100 mM CH_3COONH_4, 15 mM $(CH_3COO)_2Mg{:}4H_2O$, 20 mM
612 Tris–HCl at pH 7.6, and 6 mM 2-mercaptoethanol] and then vortexed with an
613 approximately equal volume of glass beads (212–300 mm) for 3 minutes (Merck KGaA,
614 Germany). The homogenate was centrifuged at 12,000 g for 8 min at 4 °C. The
615 supernatant was layered on top of a 5–20% linear sucrose density gradient in the
616 association buffer. It was centrifuged in an SW 41 Ti rotor (Beckman Coulter, Inc., United
617 States) at 285,000 g for 1.5 h at 4 °C. After centrifugation, the absorbance of the sucrose

618 gradient was measured at 260 nm using a UV-1800 spectrophotometer (Shimadzu Co.,
619 Japan) to obtain ribosome profiles. The 100S ribosomal fractions were identified from
620 the measured ribosomal profiles, and these fractions were stored. The solution containing
621 100S ribosomes was concentrated (final concentration: about 895 pmol), and sucrose was
622 removed using Amicon-100K (Merck KGaA, Germany).

623 ***Sample preparation and cryo-electron microscopy acquisition***

624 The ribosome complex was program-reconstructed using 1.2 μM 100S
625 hibernating ribosomes complexed with HPF and RMF from *E. coli* W3110 strain and 7.2
626 μM *E. coli* RNase I, incubated in the reaction buffer (20 mM Hepes-KOH pH 7.6, 10 mM
627 $MgOAc_2$, 30 mM NH_4Cl, 6 mM β-mercaptoethanol) at 37°C for 30 min. After 1.5-fold
628 diluting the complex, it was applied onto an EM-grid and plunge-frozen in liquid
629 nitrogen-cooled ethane. Quantifoil R2/2 gold 200 mesh grid (Quantifoil Micro Tools
630 GmbH, Germany) glow-discharged for 30 sec in a PIB-10 Ion Bombarder (Vacuum
631 Device Inc, Japan) was used to apply 2.7 μL sample, pre-incubated for 10 sec, blotted for
632 15 sec, and post-incubated for 2 sec at 4°C and 100% humidity before freezing in a
633 Vitrobot Mark IV (ThemoScientific, United States). The grids were subsequently clipped
634 into an autogrid cartridge and transferred into a CRYO ARM 300 II field emission cryo-
635 electron microscope (JEOL, Japan) operating at 300 keV, and data acquired with a K3
636 camera (Gatan, United States) using SerialEM software[78]. The cryo-EM movies were
637 acquired at a calibrated magnification of 80,460 and a pixel size of 0.87 Å/pixel to record
638 movies with 70 frames with a total accumulated dose of 50 $e^-/Å^2$/movie.

639 ***Cryo-electron microscopy image processing***

640 Image processing steps are summarized in Extended Data Fig. 3. All image
641 processing steps were performed by cryoSPARC 3.3.1 and 4.0.0 software[79]. 2,000 of

642 33,302 movies were initially motion-corrected by the patch motion correction job,
643 followed by the patch CTF estimation. 258,744 particles were picked by the circular blob,
644 which is 260 – 300 Å, using the blob picker job and extracted at a 4-fold decimated pixel
645 size (3.48 Å per pixel). The extracted particles were two-dimensional (2D) classified to
646 remove the classes of 30S subunit and debris. The 70S particles on the micrographs were
647 then re-picked at a size of 360 Å using the classes selected as templates, followed by the
648 extract from the micrographs job and 2D classification jobs. Five ab-initio volumes were
649 reconstructed using selected 146,282 particles to obtain the main class average of the 70S
650 ribosome and discard the classes of 50S subunit and debris by the heterogenous
651 refinement job. After the 70S-like particles were combined using the homogeneous
652 refinement, followed by the local refinement with signal subtraction on the 30S head, the
653 three-dimensional (3D) classification focused on the head region was performed,
654 obtaining RNase I binding particles. Selected 33,823 particles were extracted at 1.25-fold
655 decimated pixel size (2.175 Å per pixel). The complex could not find the RMF in the
656 volume at a nominal resolution of 2.8 Å. Next, the remaining movies were processed in
657 the same way as described above. The heterogeneous refinement was performed to extract
658 the 70S-like classes composed of 1,501,256 particles from the 2D classes of all 33,294
659 micrographs. The soft mask focused on the 30S head with the hibernation factors (HFs),
660 and RNase I was generated using UCSF ChimeraX 1.5[80], before 351,633 particles
661 containing hibernating 70S with RNase I were obtained by the 3D classification, followed
662 by the local refinement with signal subtraction to improve the local resolution of the
663 focused region. The local 3D volume was refined to a nominal resolution of 2.4 Å, yet
664 the density of RMF remained poor. Thereupon, two rounds of the 3D classification
665 discarded particles containing the weak density map of RMF. 3D classification using the

666 mask on the 30S platform, including S1 further sorted out 50,955 particles, including
667 RMF and part of S1. The final reconstruction was refined to a nominal resolution of 2.8
668 Å in a homogeneous map and to 2.8 Å in a local map of the mask on the 30S head, taking
669 into account the global/local CTF refinements after the particles were re-extracted at 1.4-
670 fold decimated pixel size (1.21 Å per pixel). Since the orientation of both homogeneous
671 and local volumes were slightly different, the local volume was docked into the
672 homogeneous volume using the 'Fit in Map' function and resampled to the grid of
673 homogeneous refinement using trilinear interpolation by the 'volume resample' operation
674 in ChimeraX 1.6.1[80].

675 ***Model building and refinement***

676 The *E. coli* 70S ribosome structure in this study was built in the 2.8 Å density
677 map obtained by homogeneous refinement in cryoSPARC, using a model of the *E. coli*
678 70S ribosome structure from PDB 8SYL as follows. After removing all molecules and
679 ions other than ribosome components of the 8SYL[5] model, the ribosomal subunits, split
680 into 50S and 30S using PyMOL, were docked as rigid bodies into the density map using
681 the 'Fit in Map' function in ChimeraX 1.6.1[80]. The model of each subunit was refined
682 with jelly-body restraints by Servalcat 0.4.74[81]. The models were manually corrected for
683 their ribosomal proteins according to secondary structure and Ramachandran restraints
684 for better fitting into the density map using the 'Real Space Refine Zone' function in Coot
685 0.9.8.95[82,83]. Also, nucleotides of the rRNA chains in the models were manually corrected
686 for their syn or anti-conformations with reference to the differential Fourier map produced
687 by Servalcat. The models of the HPF derived from the crystal structure of *T. thermophilus*
688 70S•*E. coli* HPF complex (PDB 4V8H[34]) and the RMF derived from the cryo-EM
689 structure of *E. coli* hibernating ribosome complex (PDB 6H4N[30]) were rigid-body fitted

690 into the homogenous density map, respectively. The crystal structure of *E. coli* RNase I
691 (PDB 2Z70[35]) was rigid-body fitted into the EM density map of the local refinement
692 focused on the 30S head region in cryoSPARC. Two mutated residues H55F and H133F
693 at the active site of the RNase I model were manually modified and corrected in Coot.
694 These models were merged into the 30S model before it was jelly-body refined by
695 Servalcat, then the 30S binding partners, especially, were manually corrected, residue by
696 residue, in Coot, together with Ramachandran and secondary structure restraints. After
697 merging the models of the 30S complex and 50S into hibernating 70S•RNase I complex,
698 a series of operations in jelly-body refinement and manual correction were repeated
699 several rounds until the model satisfied its geometry. Magnesium ions and water
700 molecules from 8SYL were docked into the model of the 70S•RNase I complex in Coot.
701 After refining the small molecules merged with the complex by Servalcat, their atomic
702 coordinates were manually corrected or removed to better fit the density map and the
703 differential Fourier map. The resulting model was validated using a comprehensive cryo-
704 EM validation tool in PHENIX 1.21.1[84,85] (Extended Data Table 1).

705 ***APBS and PISA calculations***

706 The surface potential values were produced by APBS[37]. The interfacing residues
707 and the buried surface areas were calculated using the protein interface, surfaces, and
708 assemblies (PISA) provided by Protein Data Bank Europe (PDBe)[36]
709 (https://www.ebi.ac.uk/pdbe/pisa/). Color coding based on BSA values was done on
710 PyMOL using the original Python program colorByBSA.py
711 (https://github.com/minami1009/colorByBSA).

712 ***In vitro RNA degradation and binding assays***

713 The *in vitro* assays were performed based on the previous study[33]. For the

714 inhibition assay, 0.075 pmol of the recombinant RNase I was mixed with 0.030 A_{260} of
715 crude, purified, or reconstituted ribosomes. The mixtures were incubated for 30 min and
716 30 °C, and the RNase activity of each mixture was quantified using the RNase Activity
717 Assay Kit (Abcam).

718 For the binding assay, 20 μM each of ribosomes (70S ribosome or reconstituted
719 hibernating ribosome) and RNase I mutant (H55F/H133F) was mixed and incubated for
720 30 min and 37 °C. The mixture was then loaded onto the ultrafiltration device (300,000
721 MWCO; PALL) and centrifuged at 14,000 g. Following centrifugation, the retentate and
722 the filtrate were collected separately. RNase I and the ribosomal protein in each sample
723 were detected by western blotting.

724 The binding assay following *in vitro* translation was performed as follows: *In*
725 *vitro* translation using PURE*frex* 1.0 (GeneFrontier) with or without 1 μg of pET-*gfp* as
726 a template was performed for 30 min and 37 °C. When hibernating ribosomes were used,
727 RMF and HPF were added to ribosomes before *in vitro* translation. RNase I mutant
728 (H55F/H133F) was added to the translation mixture at a final concentration of 4.8 μM
729 and incubated for a further 30 min. After ultrafiltration, the filtrate was collected, and the
730 RNase activity of the filtrate was detected as described above.

731 For the *in vitro* translation inhibition assays, *in vitro* translation was performed
732 as described above with modifications: 6 μM of RNase I mutant (H55F/H133F) was
733 added to the translation mixture with 1 μM of ribosomes at the beginning of incubation.

734 ***Single-molecule imaging analyses***

735 The translation mRNA template was transcribed from the template vector using
736 an *in vitro* transcription kit (Promega) and purified using NucleoSpin RNA
737 (MACHEREY-NAGEL). The mRNA template was hybridized with the 5′ Cy3-labeled

738 oligo DNA as follows: 1 μM of oligo DNA was denatured at 1 min and 95 °C in the
739 phosphate buffer (25 mM Na_2HPO_4, 75 mM NaH_2PO_4, 100 mM NaCl, pH 6.4), 300 nM
740 of the mRNA template was added to the mixture, and hybridization was performed by
741 lowering the temperature to 25 °C at a rate of 0.1 °C/s. The mixture was added to the
742 PURE*frex* 1.0 solution I, II, 200 nM of ribosomes, and 50 nM of HaloTag-biotin ligand.
743 The resulting solution is described as translation reaction solution A. The translation
744 reaction solution A was pre-incubated at 25 min and 30 °C.

745 Purified RNase I mutant (H55F/H133F) and nanobody of MoonTag were
746 buffered to 100 mM $NaHCO_3$, and fluorescence-labeled NHS esters (Alexa Fluor 488 for
747 nanobody of MoonTag and Alexa Fluor 660 for RNase I mutant, respectively) were added
748 and incubated at room temperature for 1 h. To remove the unreacted fluorescent dye, the
749 mixtures were ultrafiltrated using Amicon Ultra 0.5 (3,000 MWCO; Merck Millipore)
750 and purified using a gel filtration column NAP-5 (Cytiva). These fluorescence-labeled
751 proteins were added to the PURE*frex* 1.0 solution I and II at a final concentration of 250
752 nM (nanobody of MoonTag) and 20 nM (RNase I mutant), respectively. The resulting
753 solution is described as translation reaction solution B.

754 Single-molecule imaging analyses for the detection of translating ribosomes
755 were carried out as described previously[86] with the following modifications. 3 mg/mL
756 biotinylated BSA was poured into a flow cell and washed with Polymix buffer (50 mM
757 Tris-OAc (pH 7.5), 5 mM $Mg(OAc)_2$, 1 mM EDTA, 100 mM KCl, 5 mM NH_4OAc, 0.5
758 mM $Ca(OAc)_2$, 5 mM putrescine, 1 mM spermidine, 5 mM β-mercaptoethanol)
759 containing 0.2% Tween 20. After blocking, 0.33 mg/mL streptavidin was loaded,
760 followed by washing with Polymix buffer. After streptavidin treatment, 10 μL of
761 translation reaction solution A, which was pre-incubated at 30°C for 25 min, was loaded,

762 followed by washing with Polymix buffer twice. At last, translation reaction solution B
763 containing fluorescence-labeled RNase I mutant (H55F/H133F) and nanobody was added
764 into the flow cell, and the flow cell was sealed. The flow cell was placed on inverted
765 microscopy (Nikon), and Alexa Fluor 488, Cy3, and Alexa Fluor 660 fluorescences were
766 detected upon 488, 532, and 647 nm excitation, respectively. The images were analyzed
767 with TrackMate plugin of Fiji, after background subtraction. Analysis of the tracking data
768 and creation of figures were performed using an original Python program.

769 ***In vivo trans-translation activity assays***

770 The *trans*-translation activity in *E. coli* cells was quantified based on the
771 previous research[87]. In brief, *E. coli* Δ*ssrA* or Δ*ssrA*Δ*rna* cells harboring pMW-*ssrA*^{DD}
772 and pAcGFP-woSTOP-*trpAt* were cultivated in L-broth at 37 °C until an OD660 reached
773 0.3, IPTG was added to the culture at a final condition of 1 mM and further cultivated for
774 1.5 h. The culture was collected and resuspended in PBS, and GFP intensity was
775 quantified.

776 ***In vitro rRNA degradation from split ribosome subunits***

777 The susceptibility of rRNA to degradation by RNase I was compared for rRNA
778 derived from 70S ribosomes and 30S/50S subunits. The dissociation of 70S ribosomes
779 into 30S/50S subunits was performed as follows[48]: 20 pmol of ribosomes was
780 resuspended to the prokaryotic ribosome dissociation buffer (10 mM Tris-HCl (pH 7.5),
781 1 mM $Mg(OAc)_2$, 100 mM NH_4Cl, 1 mM DTT, 0.5 mM EDTA) and allowed to stand
782 overnight at 4 °C. 124 pmol of RNase I was added to the solution and incubated for 30
783 min and 37 °C, and rRNA was extracted using RNeasy Mini Kit as described above. The
784 rRNAs were detected with electrophoresis using MOPS-formaldehyde denaturing gel.

785 ***Preparation of figures***

786 All figures were generated by PyMOL (The PyMOL Molecular Graphics System,
787 Version 3.0.0 Schrödinger, LLC), Chimera X 1.7.1, Matplotlib (Version 3.7.1), and
788 Seaborn (Version 0.13.1) libraries of Python (Version 3.10.12), OmniGraffle, and
789 Affinity Designer (Version 1.10.5).
790
791 **Data availability**
792 The atomic coordinate of hibernating 70S ribosome in complex with RNase I
793 mutant was deposited in the Protein Data Bank Japan (PDBj) under accession code 9IOT.
794 The cryo-EM map was deposited in the Electron Microscopy Data Bank (EMDB) under
795 accession code EMD-60747, and the local map focused on the 30S head was deposited
796 as an additional map.
797
798 **Acknowledgments**
799 We thank K. Namba, T. Miyata, and F. Makino for their work supporting the
800 cryo-EM facility of Osaka University; the members of the Laboratory for Cryo-EM
801 structural biology (the T. Kato group) for supporting and advising the cryo-EM single
802 particle analysis; K. Yamashita for advising model refinement using Servalcat; T. Suzuki,
803 A. Nagao and N. Akiyama for performing the SDGC and the isolation of ribosomes; W.
804 Fujii for providing the plasmid encoding the antibody of MoonTag; and H. Himeno for
805 providing the plasmid pMW-ssrA^{DD}. This work was financed by the JSPS KAKENHI
806 (Grant numbers 20K21266 and 23H02122) to T.O. and by JST SPRING (Grant number
807 JPMJSP2108) to A.M. This research was [partially] supported by Research Support
808 Project for Life Science and Drug Discovery (Basis for Supporting Innovative Drug
809 Discovery and Life Science Research (BINDS)) from AMED under Grant Number

JP23ama121001.

Author contributions

A.M. performed biochemical assays. A.M., T.T. and H.Y. prepared cryo-EM samples. T.T. prepared cryo-EM grids, collected cryo-EM data, and generated and refined the molecular models. Z.Y. and T.F. prepared the microscopy. A.M. and Z.Y. performed the single-molecule imaging assays and analyses. A.M., T.T., Ta.K., To.K. and T.O. analysed and interpreted data. A.M. and T.T. prepared the figures and tables. A.M., T.T. and T.O. wrote the manuscript. T.O. conceived and supervised the project. All authors discussed and commented on the final manuscript.

Corresponding authors

Correspondence to Tetsuhiro Ogawa (atetsu@g.ecc.u-tokyo.ac.jp) or Takehito Tanzawa (takehito.tanzawa@protein.osaka-u.ac.jp).

Competing interest declaration

The authors declare no competing interests.

References

1. Irving, S. E., Choudhury, N. R. & Corrigan, R. M. The stringent response and physiological roles of (pp)pGpp in bacteria. *Nat. Rev. Microbiol.* **19**, 256–271 (2021).
2. Bechhofer, D. H. & Deutscher, M. P. Bacterial ribonucleases and their roles in RNA metabolism. *Crit. Rev. Biochem. Mol. Biol.* **54**, 242–300 (2019).
3. Sulthana, S., Basturea, G. N. & Deutscher, M. P. Elucidation of pathways of ribosomal

RNA degradation: an essential role for RNase E. *RNA* **22**, 1163–1171 (2016).

4. Jacob, A. I., Köhrer, C., Davies, B. W., RajBhandary, U. L. & Walker, G. C. Conserved bacterial RNase YbeY plays key roles in 70S ribosome quality control and 16S rRNA maturation. *Mol. Cell* **49**, 427–438 (2013).

5. Cheng, Z.-F. & Deutscher, M. P. Quality control of ribosomal RNA mediated by polynucleotide phosphorylase and RNase R. *Proc. Natl. Acad. Sci. U. S. A.* **100**, 6388–6393 (2003).

6. Prossliner, T., Skovbo Winther, K., Sørensen, M. A. & Gerdes, K. Ribosome Hibernation. *Annu. Rev. Genet.* **52**, 321–348 (2018).

7. Wada, A., Yamazaki, Y., Fujita, N. & Ishihama, A. Structure and probable genetic location of a "ribosome modulation factor" associated with 100S ribosomes in stationary-phase Escherichia coli cells. *Proc. Natl. Acad. Sci. U. S. A.* **87**, 2657–2661 (1990).

8. Wada, A., Igarashi, K., Yoshimura, S., Aimoto, S. & Ishihama, A. Ribosome modulation factor: stationary growth phase-specific inhibitor of ribosome functions from Escherichia coli. *Biochem. Biophys. Res. Commun.* **214**, 410–417 (1995).

9. Prossliner, T., Gerdes, K., Sørensen, M. A. & Winther, K. S. Hibernation factors directly block ribonucleases from entering the ribosome in response to starvation. *Nucleic Acids Res.* **49**, 2226–2239 (2021).

10. Lipońska, A. & Yap, M.-N. F. Hibernation-Promoting Factor Sequesters Staphylococcus aureus Ribosomes to Antagonize RNase R-Mediated Nucleolytic Degradation. *MBio* **12**, e0033421 (2021).

11. Helena-Bueno, K. *et al.* A new family of bacterial ribosome hibernation factors. *Nature* **626**, 1125–1132 (2024).

12. Van Dyke, N., Baby, J. & Van Dyke, M. W. Stm1p, a ribosome-associated protein, is important for protein synthesis in Saccharomyces cerevisiae under nutritional stress conditions. *J. Mol. Biol.* **358**, 1023–1031 (2006).

860 13. Wang, Y. J. *et al.* Lso2 is a conserved ribosome-bound protein required for translational
861 recovery in yeast. *PLoS Biol.* **16**, e2005903 (2018).
862 14. Andersen, K. L. & Collins, K. Several RNase T2 enzymes function in induced tRNA and
863 rRNA turnover in the ciliate Tetrahymena. *Mol. Biol. Cell* **23**, 36–44 (2012).
864 15. Hillwig, M. S. *et al.* RNS2, a conserved member of the RNase T2 family, is necessary for
865 ribosomal RNA decay in plants. *Proc. Natl. Acad. Sci. U. S. A.* **108**, 1093–1098 (2011).
866 16. Haud, N. *et al. rnaset2* mutant zebrafish model familial cystic leukoencephalopathy and
867 reveal a role for RNase T2 in degrading ribosomal RNA. *Proceedings of the National*
868 *Academy of Sciences* **108**, 1099–1103 (2011).
869 17. Sato, K. & Egami, F. STUDIES ON RIBONUCLEASES IN TAKADIASTASE. I. *J.*
870 *Biochem.* **44**, 753–767 (1957).
871 18. Luhtala, N. & Parker, R. T2 Family ribonucleases: ancient enzymes with diverse roles.
872 *Trends Biochem. Sci.* **35**, 253–259 (2010).
873 19. Huang, H. *et al.* Bulk RNA degradation by nitrogen starvation-induced autophagy in yeast.
874 *EMBO J.* **34**, 154–168 (2015).
875 20. Minami, A. *et al.* RNase T2-involved selective autophagy of ribosomes induced by
876 starvation in yeast. *bioRxiv* 2023.07.14.548783 (2023) doi:10.1101/2023.07.14.548783.
877 21. Henneke, M. *et al.* RNASET2-deficient cystic leukoencephalopathy resembles congenital
878 cytomegalovirus brain infection. *Nat. Genet.* **41**, 773–775 (2009).
879 22. Greulich, W. *et al.* TLR8 Is a Sensor of RNase T2 Degradation Products. *Cell* **179**, 1264-
880 1275.e13 (2019).
881 23. Takayama, S. & Isogai, A. Self-incompatibility in plants. *Annu. Rev. Plant Biol.* **56**, 467–
882 489 (2005).
883 24. Beppu, T. & Arima, K. Induction by mercuric ion of extensive degradation of cellular
884 ribonucleic acid in Escherichia coli. *J. Bacteriol.* **98**, 888–897 (1969).
885 25. Meador, J., 3rd & Kennell, D. Cloning and sequencing the gene encoding Escherichia coli

886 ribonuclease I: exact physical mapping using the genome library. *Gene* **95**, 1–7 (1990).
887 26. Neu, H. C. & Heppel, L. A. THE RELEASE OF RIBONUCLEASE INTO THE
888 MEDIUM WHEN ESCHERICHIA COLI CELLS ARE CONVERTED TO
889 SPEROPLASTS. *J. Biol. Chem.* **239**, 3893–3900 (1964).
890 27. Datta, A. K. & Burma, D. P. Association of ribonuclease I with ribosomes and their
891 subunits. *J. Biol. Chem.* **247**, 6795–6801 (1972).
892 28. Flemming, H.-C. & Wuertz, S. Bacteria and archaea on Earth and their abundance in
893 biofilms. *Nat. Rev. Microbiol.* **17**, 247–260 (2019).
894 29. Ueta, M. *et al.* Ribosome binding proteins YhbH and YfiA have opposite functions during
895 100S formation in the stationary phase of Escherichia coli. *Genes Cells* **10**, 1103–1112
896 (2005).
897 30. Beckert, B. *et al.* Structure of a hibernating 100S ribosome reveals an inactive
898 conformation of the ribosomal protein S1. *Nature Microbiology* **3**, 1115–1121 (2018).
899 31. Maruyama, H. & Mizuno, D. The participation of ribonuclease in the degradation of
900 Escherichia coli ribosomal ribonucleic acid as revealed by oligonucleotides accumulation
901 in the phorphorus-deficient stage. *Biochim. Biophys. Acta* **108**, 593–604 (1965).
902 32. Wade, H. E., Lovett, S. & Robinson, H. K. The autodegradation of 32-P-labelled
903 ribosomes from Escherichia coli. *Biochem. J* **93**, 121–128 (1964).
904 33. Kitahara, K. & Miyazaki, K. Specific inhibition of bacterial RNase T2 by helix 41 of 16S
905 ribosomal RNA. *Nat. Commun.* **2**, 1–7 (2011).
906 34. Polikanov, Y. S., Blaha, G. M. & Steitz, T. A. How Hibernation Factors RMF, HPF, and
907 YfiA Turn Off Protein Synthesis. *Science* **336**, 915–918 (2012).
908 35. Rodriguez, S. M. *et al.* Nonspecific base recognition mediated by water bridges and
909 hydrophobic stacking in ribonuclease I from Escherichia coli. *Protein Sci.* **17**, 681–690
910 (2008).
911 36. Krissinel, E. & Henrick, K. Inference of macromolecular assemblies from crystalline state.

912 *J. Mol. Biol.* **372**, 774–797 (2007).
913 37. Jurrus, E. *et al.* Improvements to the APBS biomolecular solvation software suite. *Protein*
914 *Sci.* **27**, 112–128 (2018).
915 38. Seely, S. M. *et al.* Molecular basis of the pleiotropic effects by the antibiotic amikacin on
916 the ribosome. *Nat. Commun.* **14**, 4666 (2023).
917 39. Shimizu, Y. *et al.* Cell-free translation reconstituted with purified components. *Nat.*
918 *Biotechnol.* **19**, 751–755 (2001).
919 40. Wu, B., Eliscovich, C., Yoon, Y. J. & Singer, R. H. Translation dynamics of single
920 mRNAs in live cells and neurons. *Science* **352**, 1430–1435 (2016).
921 41. Morisaki, T. *et al.* Real-time quantification of single RNA translation dynamics in living
922 cells. *Science* **352**, 1425–1429 (2016).
923 42. Yan, X., Hoek, T. A., Vale, R. D. & Tanenbaum, M. E. Dynamics of Translation of Single
924 mRNA Molecules In Vivo. *Cell* **165**, 976–989 (2016).
925 43. Wang, C., Han, B., Zhou, R. & Zhuang, X. Real-Time Imaging of Translation on Single
926 mRNA Transcripts in Live Cells. *Cell* **165**, 990–1001 (2016).
927 44. Fontaine, B. M. *et al.* RNase I regulates Escherichia coli 2',3'-cyclic nucleotide
928 monophosphate levels and biofilm formation. *Biochem. J* **475**, 1491–1506 (2018).
929 45. Deutscher, Murray P. Chapter 9 Maturation and Degradation of Ribosomal RNA in
930 Bacteria. in *Progress in Molecular Biology and Translational Science* vol. 85 369–391
931 (Academic Press, 2009).
932 46. Zundel, M. A., Basturea, G. N. & Deutscher, M. P. Initiation of ribosome degradation
933 during starvation in Escherichia coli. *RNA* **15**, 977–983 (2009).
934 47. Himeno, H., Nameki, N., Kurita, D., Muto, A. & Abo, T. Ribosome rescue systems in
935 bacteria. *Biochimie* **114**, 102–112 (2015).
936 48. Rivera, M. C., Maguire, B. & Lake, J. A. Dissociation of ribosomes into large and small
937 subunits. *Cold Spring Harb. Protoc.* **2015**, 363–367 (2015).

938 49. Keiler, K. C. Mechanisms of ribosome rescue in bacteria. *Nat. Rev. Microbiol.* **13**, 285–
939 297 (2015).
940 50. Paier, A., Leppik, M., Soosaar, A., Tenson, T. & Maiväli, Ü. The effects of disruptions in
941 ribosomal active sites and in intersubunit contacts on ribosomal degradation in Escherichia
942 coli. *Sci. Rep.* **5**, 7712 (2015).
943 51. Ron, E. Z. Polysome turnover during amino acid starvation in Escherichia coli. *J.*
944 *Bacteriol.* **108**, 263–268 (1971).
945 52. Cozzone, A. J. How do bacteria synthesize proteins during amino acid starvation? *Trends*
946 *Biochem. Sci.* **6**, 108–110 (1981).
947 53. Fessler, M., Gummesson, B., Charbon, G., Svenningsen, S. L. & Sørensen, M. A. Short-
948 term kinetics of rRNA degradation in Escherichia coli upon starvation for carbon, amino
949 acid or phosphate. *Mol. Microbiol.* **113**, 951–963 (2020).
950 54. Filbeck, S., Cerullo, F., Pfeffer, S. & Joazeiro, C. A. P. Ribosome-associated quality-
951 control mechanisms from bacteria to humans. *Mol. Cell* **82**, 1451–1466 (2022).
952 55. Saito, K. *et al.* Ribosome collisions induce mRNA cleavage and ribosome rescue in
953 bacteria. *Nature* **603**, 503–508 (2022).
954 56. LaRiviere, F. J., Cole, S. E., Ferullo, D. J. & Moore, M. J. A late-acting quality control
955 process for mature eukaryotic rRNAs. *Mol. Cell* **24**, 619–626 (2006).
956 57. Cole, S. E., LaRiviere, F. J., Merrikh, C. N. & Moore, M. J. A convergence of rRNA and
957 mRNA quality control pathways revealed by mechanistic analysis of nonfunctional rRNA
958 decay. *Mol. Cell* **34**, 440–450 (2009).
959 58. Garza-Sánchez, F., Gin, J. G. & Hayes, C. S. Amino acid starvation and colicin D
960 treatment induce A-site mRNA cleavage in Escherichia coli. *J. Mol. Biol.* **378**, 505–519
961 (2008).
962 59. Messens, J. *et al.* The Oxidase DsbA Folds a Protein with a Nonconsecutive Disulfide*. *J.*
963 *Biol. Chem.* **282**, 31302‑31307 (2007).

964 60. Padmanabhan, S., Zhou, K., Chu, C. Y., Lim, R. W. & Lim, L. W. Overexpression,
965 biophysical characterization, and crystallization of ribonuclease I from Escherichia coli, a
966 broad-specificity enzyme in the RNase T2 family. *Arch. Biochem. Biophys.* **390**, 42–50
967 (2001).
968 61. Ohnishi, Y., Iguma, H., Ono, T., Nagaishi, H. & Clark, A. J. Genetic mapping of the F
969 plasmid gene that promotes degradation of stable ribonucleic acid in Escherichia coli. *J.*
970 *Bacteriol.* **132**, 784–789 (1977).
971 62. Onishi, Y. F factor promotes turnover of stable RNA in escherichia coli. *Science* **187**,
972 257–258 (1975).
973 63. Gao, H. *et al.* Study of the structural dynamics of the E coli 70S ribosome using real-space
974 refinement. *Cell* **113**, 789–801 (2003).
975 64. Yapici, I. *et al.* 4D Crystallography Captures Transient IF1-Ribosome Dynamics in
976 Translation Initiation. *bioRxiv* 2023.10.27.564398 (2023) doi:10.1101/2023.10.27.564398.
977 65. Akanuma, G. *et al.* Evolution of Ribosomal Protein S14 Demonstrated by the
978 Reconstruction of Chimeric Ribosomes in Bacillus subtilis. *J. Bacteriol.* **203**, (2021).
979 66. Xaplanteri, M. A., Papadopoulos, G., Leontiadou, F., Choli-Papadopoulou, T. & Kalpaxis,
980 D. L. The contribution of the zinc-finger motif to the function of Thermus thermophilus
981 ribosomal protein S14. *J. Mol. Biol.* **369**, 489–497 (2007).
982 67. Li, Y. *et al.* Zinc depletion induces ribosome hibernation in mycobacteria. *Proc. Natl.*
983 *Acad. Sci. U. S. A.* **115**, 8191–8196 (2018).
984 68. Thorn, A. *et al.* Structure and activity of the only human RNase T2. *Nucleic Acids Res.* **40**,
985 8733–8742 (2012).
986 69. Dimitrova-Paternoga, L. *et al.* Structural basis of ribosomal 30S subunit degradation by
987 RNase R. *Nature* **626**, 1133–1140 (2024).
988 70. Baba, T. *et al.* Construction of Escherichia coli K-12 in-frame, single-gene knockout
989 mutants: the Keio collection. *Mol. Syst. Biol.* **2**, 2006.0008 (2006).

990 71. Boersma, S. *et al.* Multi-Color Single-Molecule Imaging Uncovers Extensive
991 Heterogeneity in mRNA Decoding. *Cell* **178**, 458-472.e19 (2019).
992 72. Yang, Z., Iizuka, R. & Funatsu, T. Nascent SecM chain outside the ribosome reinforces
993 translation arrest. *PLoS One* **10**, e0122017 (2015).
994 73. Dijk, J. & Littlechild, J. Purification of ribosomal proteins from Escherichia coli under
995 nondenaturing conditions. *Methods Enzymol.* **59**, 481–502 (1979).
996 74. Akiyama, N. *et al.* Structural insights into the decoding capability of isoleucine tRNAs
997 with lysidine and agmatidine. *Nat. Struct. Mol. Biol.* **31**, 817–825 (2024).
998 75. Feaga, H. A., Kopylov, M., Kim, J. K., Jovanovic, M. & Dworkin, J. Ribosome
999 Dimerization Protects the Small Subunit. *J. Bacteriol.* **202**, (2020).
1000 76. Minami, A. *et al.* Establishment of the improved colonization of Escherichia coli
1001 laboratory strain in the intestine mediated by single gene deletion. *Biochem. Biophys. Res.*
1002 *Commun.* 150448 (2024).
1003 77. Vogel, H. J. & Bonner, D. M. ACETYLORNITHINASE OF ESCHERICHIA COLI:
1004 PARTIAL PURIFICATION AND SOME PROPERTIES. *J. Biol. Chem.* **218**, 97–106
1005 (1956).
1006 78. Mastronarde, D. N. Automated electron microscope tomography using robust prediction of
1007 specimen movements. *J. Struct. Biol.* **152**, 36–51 (2005).
1008 79. Punjani, A., Rubinstein, J. L., Fleet, D. J. & Brubaker, M. A. cryoSPARC: algorithms for
1009 rapid unsupervised cryo-EM structure determination. *Nat. Methods* **14**, 290–296 (2017).
1010 80. Pettersen, E. F. *et al.* UCSF ChimeraX: Structure visualization for researchers, educators,
1011 and developers. *Protein Sci.* **30**, 70–82 (2021).
1012 81. Yamashita, K., Palmer, C. M., Burnley, T. & Murshudov, G. N. Cryo-EM single-particle
1013 structure refinement and map calculation using Servalcat. *Acta Crystallogr D Struct Biol*
1014 **77**, 1282–1291 (2021).
1015 82. Emsley, P., Lohkamp, B., Scott, W. G. & Cowtan, K. Features and development of Coot.

1016 *Acta Crystallogr. D Biol. Crystallogr.* **66**, 486–501 (2010).
1017 83. Casañal, A., Lohkamp, B. & Emsley, P. Current developments in Coot for macromolecular
1018 model building of Electron Cryo-microscopy and Crystallographic Data. *Protein Sci.* **29**,
1019 1069–1078 (2020).
1020 84. Liebschner, D. *et al.* Macromolecular structure determination using X-rays, neutrons and
1021 electrons: recent developments in Phenix. *Acta Crystallogr D Struct Biol* **75**, 861–877
1022 (2019).
1023 85. Chen, V. B. *et al.* MolProbity: all-atom structure validation for macromolecular
1024 crystallography. *Acta Crystallogr. D Biol. Crystallogr.* **66**, 12–21 (2010).
1025 86. Masuda, T. *et al.* Initiation factor 2, tRNA, and 50S subunits cooperatively stabilize
1026 mRNAs on the ribosome during initiation. *Proc. Natl. Acad. Sci. U. S. A.* **109**, 4881–4885
1027 (2012).
1028 87. Ramadoss, N. S. *et al.* Small molecule inhibitors of *trans*-translation have broad-spectrum
1029 antibiotic activity. *Proc. Natl. Acad. Sci. U. S. A.* **110**, 10282–10287 (2013).
1030